

Improvement of energy resolution of x-ray transition-edge sensor using K-means algorithm and Wiener filter

Qingxiao Ma(马卿效), Wen Zhang(张文), Peizhan Li(李佩展), Zheng Wang(王争), Zhifa Feng(冯志发), Xinkai Yang(杨心开), Jiaqiang Zhong(钟家强), Wei Miao(缪巍), Yuan Ren(任远), Jing Li(李婧), and Shengcai Shi(史生才)
Citation: Chin. Phys. B, 2023, 32 (**10**): 108501. DOI: 10.1088/1674-1056/acd7d4
Journal homepage: http://cpb.iphy.ac.cn; http://iopscience.iop.org/cpb

What follows is a list of articles you may be interested in

Transition-edge sensors using Mo/Au/Au tri-layer films

Hubing Wang(王沪兵), Yue Lv(吕越), Dongxue Li(李冬雪), Yue Zhao(赵越), Bo Gao(高波), and Zhen Wang(王镇)
Chin. Phys. B, 2023, 32 (**2**): 028501. DOI: 10.1088/1674-1056/ac7f94

Development of series SQUID array with on-chip filter for TES detector

Wentao Wu(伍文涛), Zhirong Lin(林志荣), Zhi Ni(倪志), Peizhan Li(李佩展), Tiantian Liang(梁恬恬), Guofeng Zhang(张国峰), Yongliang Wang(王永良), Liliang Ying(应利良), Wei Peng(彭炜), Wen Zhang(张文), Shengcai Shi(史生才), Lixing You(尤立星), and Zhen Wang(王镇)
Chin. Phys. B, 2022, 31 (**2**): 028504. DOI: 10.1088/1674-1056/ac2b91

Temperature and current sensitivity extraction of optical superconducting transition-edge sensors based on a two-fluid model

Yue Geng(耿悦), Pei-Zhan Li(李佩展), Jia-Qiang Zhong(钟家强), Wen Zhang(张文), Zheng Wang(王争), Wei Miao(缪巍), Yuan Ren(任远), and Sheng-Cai Shi(史生才)
Chin. Phys. B, 2021, 30 (**9**): 098501. DOI: 10.1088/1674-1056/ac11ce

Fabrication and characterization of all-Nb lumped-element Josephson parametric amplifiers

Hang Xue(薛航), Zhirong Lin(林志荣), Wenbing Jiang(江文兵), Zhengqi Niu(牛铮琦), Kuang Liu(刘匡), Wei Peng(彭炜), and Zhen Wang(王镇)
Chin. Phys. B, 2021, 30 (**6**): 068503. DOI: 10.1088/1674-1056/abeee6

Optical response of Al/Ti bilayer transition edge sensors

Zhang Qing-Ya (张青雅), Wang Tian-Shun (王天顺), Liu Jian-She (刘建设), Dong Wen-Hui (董文慧), He Gen-Fang (何根芳), Li Tie-Fu (李铁夫), Zhou Xing-Xiang (周幸祥), Chen Wei (陈炜)
Chin. Phys. B, 2014, 23 (**11**): 118502. DOI: 10.1088/1674-1056/23/11/118502

Improvement of energy resolution of x-ray transition-edge sensor using K-means algorithm and Wiener filter

Qingxiao Ma(马卿效)[1,2], Wen Zhang(张文)[1,†], Peizhan Li(李佩展)[1,2], Zheng Wang(王争)[1], Zhifa Feng(冯志发)[1,2], Xinkai Yang(杨心开)[1,2], Jiaqiang Zhong(钟家强)[1], Wei Miao(缪巍)[1], Yuan Ren(任远)[1], Jing Li(李婧)[1], and Shengcai Shi(史生才)[1]

[1] *Purple Mountain Observatory, Chinese Academic of Sciences, Nanjing* 210023, *China*
[2] *College of Astronomy and Space Science, University of Science and Technology of China, Hefei* 230026, *China*

(Received 13 April 2023; revised manuscript received 11 May 2023; accepted manuscript online 23 May 2023)

We develop an x-ray Ti/Au transition-edge sensor (TES) with an Au absorber deposited on the center of TES and improved its energy resolution using the K-means clustering algorithm in combination with Wiener filter. We firstly extract the main parameters of each recorded pulse trace, which are adopted to classify these traces into several clusters in the K-means clustering algorithm. Then real traces are selected for energy resolution analysis. Following the baseline correction, the Wiener filter is used to improve the signal-to-noise ratio. Although the silicon underneath the TES has not been etched to reduce the thermal conductance, the energy resolution of the developed x-ray TES is improved from 94 eV to 44 eV at 5.9 keV.

Keywords: transition-edge sensors, energy resolution, K-means clustering, Wiener filter

PACS: 85.25.Oj, 85.25.Am **DOI:** 10.1088/1674-1056/acd7d4

1. Introduction

Superconducting transition-edge sensors (TESs) are extremely sensitive thermal detectors because of their sharp superconducting-to-normal transition, which can be used to detect photons from millimeter, near infrared through x-rays and γ-rays.[1] Large-format TES arrays with higher energy resolution (ΔE) are widely used in the fields of astrophysics and particle physics. For example, Athena x-ray observatory proposed by ESA is planned to launch in the 2030s. The x-ray integral field unit (X-IFU) on board of Athena is a cryogenic imaging spectrometer based on several thousands of TESs with ΔE better than 2.5 eV for photon energies up to 7 keV.[2] Ti/Au bilayer TES microcalorimeter exhibits a ΔE of 2.0 eV@5.9 keV.[3] By reducing critical temperature (T_C) and pixel size, the best ΔE obtained up to date is 1.56 eV@5.9 keV.[4] A new process is developed to fabricate Mo/Cu bilayer TESs by breaking vacuum and introducing a patterning step between the deposition of the superconductor and normal metal layers, which can tune T_C across a broad range.[5] TES fabrication process can be simplified by integrating the sensor patterning with the deposition of Mo/Au/Au trilayer films, and ΔE of 6.66 eV@5.9 keV is reported.[6] A 4×4 Mo/Cu TES array integrated with a 2.4-μm-thick bismuth absorber has been developed for the free-electron laser facility around ShanghaiTech University, which shows a quantum efficiency of 70% and ΔE of 5.2 eV at 5.9 keV.[7] In addition, the data acquisition and processing are also crucial for obtaining better ΔE.[8] During the experiment, some false traces are recorded due to interferences, SQUID flux jump, heat sink temperature drift, high energy particle, etc., therefore it is necessary to discriminate them from the correct traces.

We have developed optical/near infrared superconducting single-photon detectors based on titanium TES,[9] whose system quantum detection efficiency is as high as 90% at telecommunication band. We further fabricate x-ray Ti/Au TES and deposit an Au absorber on the center of TES by electron-beam evaporation. Note that for the first step the silicon substrate underneath the TES sensor has not been etched. We propose to classify the recorded pulse traces into several clusters with K-means clustering algorithm, among which the correct traces are selected for the following processing. Then the baseline is corrected, followed by Wiener filtering to improve the signal-to-noise ratio, thus ΔE. As a concept of proof, we found that the ΔE of the Ti/Au TES without deep reactive ion etching (DRIE) is improved to 44 eV from its original 94 eV at 5.9 keV.

2. Transition edge sensor and measurement setup

Superconducting Ti (35 nm)/Au(50 nm) bilayer is deposited on the silicon substrate coated with a thin layer SiO_x using electron-beam evaporation in an ultrahigh vacuum environment.[10] The active area ranging from 50×50 μm^2 to 200×200 μm^2 is formed with lift-off process. A typical TES is shown in Fig. 1(a), the Ti/Au sensor is 50 μm square, and a 1.1-μm-thick gold layer with dimensions of 30×40 μm^2 is directly deposited on the Ti/Au sensor as the absorber.[11] Contact pads and wires are formed from a 150-nm-thick Nb

†Corresponding author. E-mail: wzhang@pmo.ac.cn

© 2023 Chinese Physical Society and IOP Publishing Ltd

film, whose critical temperature is 9.2 K, acting as Andreev reflection to prevent the relaxation of thermal energy. Note that the silicon substrate is not removed by DRIE and the electron-phonon interaction is the dominant energy relaxation mechanism. As shown in Fig. 1(b), the Ti/Au TES and SQUID array are mounted in a cooper block, and the TES is connected to the input inductance of the SQUID array with a current noise of 7 pA·Hz$^{-1/2}$.[12] X-ray from a ^{55}Fe source in a Pb box is incident on the TES through a 0.5 mm hole. ^{55}Fe nucleus becomes ^{55}Mn and emits an x-ray photon. The emitted x-rays are 90% ^{55}Mn K_α (5.9 keV) and 10% ^{55}Mn K_β (6.5 keV).[13] As shown in Fig. 1(c), the TES block is then anchored to the FAA stage of an adiabatic demagnetization refrigerator (ADR), whose base temperature is about 50 mK. Figure 1(d) shows the schematic diagram of the readout circuit, where $R_{\rm PAR}$ is the parasitic resistance and $I_{\rm BIAS}$ is the bias current. A shunt resistor ($R_{\rm SH}$) of 1.2 mΩ integrated in the SQUID chip provides voltage bias to the TES. The induced pulse response is recorded by a Keysight Infiniium S-series oscilloscope with the data sampling rate of 125 Ms/s.

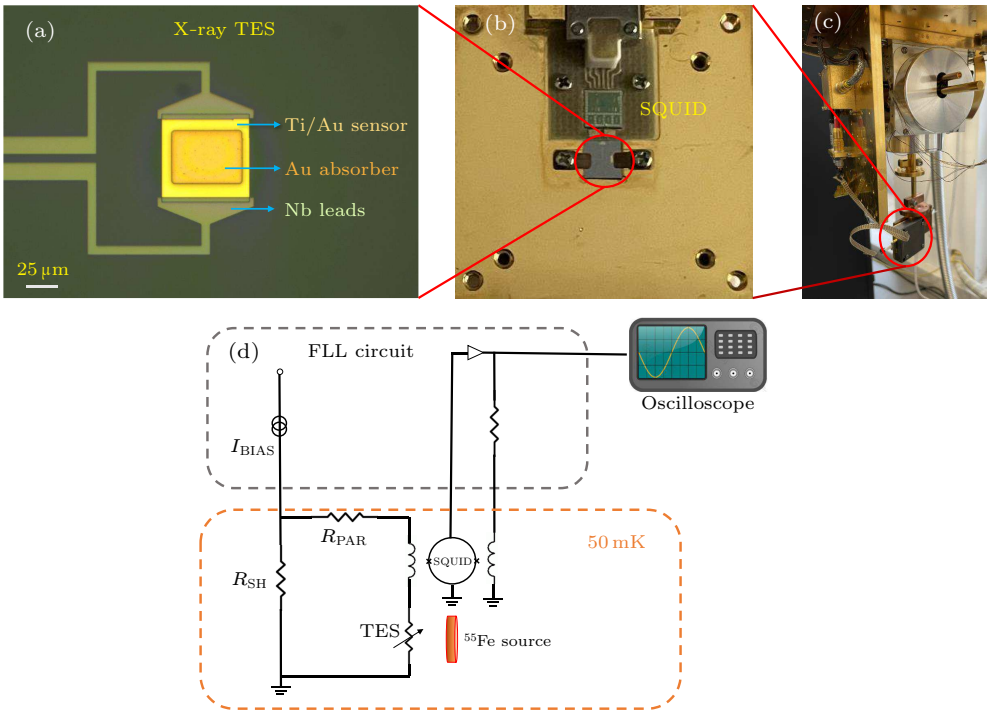


Fig. 1. X-ray superconducting TES and measurement setup: (a) photo of x-ray TES with the Au absorber on the center of Ti/Au TES, (b) x-ray TES block integrated with SQUID, (c) measurement setup in ADR refrigerator, (d) schematic diagram of the readout circuit.

We measured the resistance transition curve and current-voltage curves of the x-ray TES at different bath temperatures ($T_{\rm bath}$). Its normal resistance ($R_{\rm N}$) is 46 mΩ and critical temperature ($T_{\rm C}$) is 200 mK. The Joule power at 30% $R_{\rm N}$ is fitted to the heat flow equation,[1] and the obtained thermal conductance G is 7.7 nW/K. All key parameters for this TES are listed in Table 1.

Table 1. Main parameters of the x-ray TES.

Parameters	Values
Normal resistance	46 mΩ
Critical temperature	200 mK
Thermal conductance	7.7 nW/K

3. Pulse trace classification and baseline correction

We record 4000 pulse traces while the TES is biased at 21% $R_{\rm N}$ and $T_{\rm bath}$ of 100 mK. ^{55}Fe x-ray source has two main emission peaks, which are Mn K_α at 5.9 keV and Mn K_β at 6.5 keV. The pulse height presents the energy of absorbed x-ray photons. Figure 2 shows the energy spectra of originally recorded pulse traces. ΔE (i.e., the full width at half maximum) is 94 eV for the 5.9 keV energy peak.

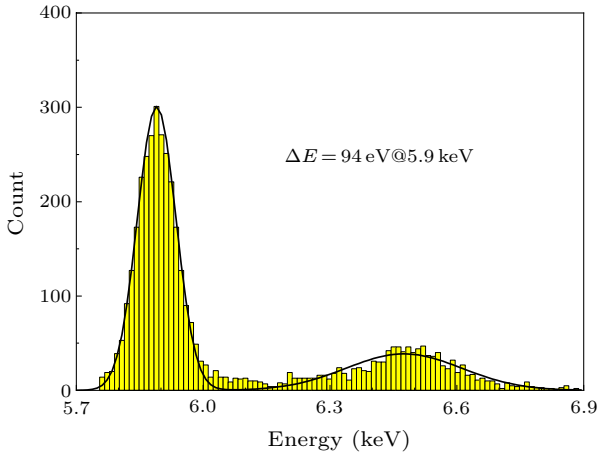


Fig. 2. The energy spectra of directly recorded x-ray pulses.

There are various noises or interferences during the experimental process. Three major noises are considered: Johnson noise and thermal fluctuation noise of the TES, and Johnson noise of $R_{\rm SH}$.[1] In addition, the switch of our water chiller for the ADR refrigerator might trigger the oscilloscope to produce false pulses. The baseline might be shifted due to SQUID flux jump. High energy particle will generate a pulse with high amplitude. Pile-up event can occur if two or more x-ray photons are incident on the TES in a short time less than the recovering time. Therefore, it is necessary to identify them and to reject the false data before further processing. To reduce the difficulty of data processing, we extract the main features of each trace. As shown in Fig. 3, a typical pulse trace includes the following features: pulse amplitude, baseline, rising edge time ($\tau_{\rm rise}$), falling edge time ($\tau_{\rm fall}$).

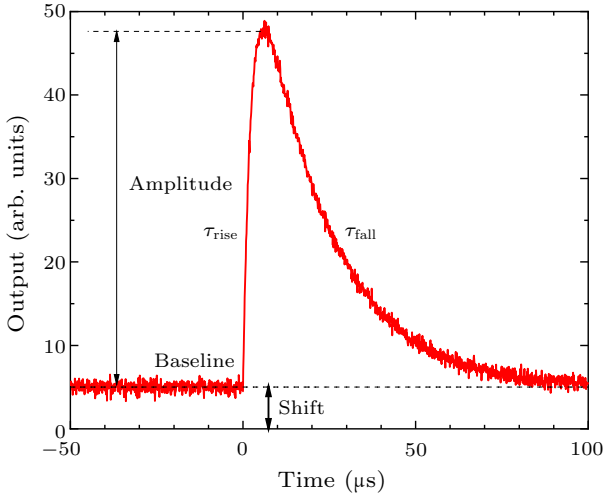


Fig. 3. Schematic diagram of response characteristics involved in K-means clustering.

Table 2. Classification of recorded pulse traces.

Cluster	Features	Possible reason	Percentage (%)
a	interference	water chiller on/off	2.2
b	baseline up shifted	SQUID flux jump	24.7
c	baseline down shifted	SQUID flux jump	27.7
d	correct pulse trace		37.7
e	pipe-up	two x-ray photons incident in a short time	2.5
f	extreme high amplitude	high energy particle	4.7
g	extreme large $\tau_{\rm fall}$	photon incident on leads	0.5

We thus divide all recorded pulse traces into 7 classes using the K-means clustering algorithm[14] as shown in Table 2. The clusters minimize the sum of the squared deviation of each pulse traces from the mean in the cluster.[15] It can be viewed as the minimization of an objective function

$$SSE = \sum_{k=1}^{K} \sum_{i \in C_k} \sum_{j=1}^{4} (x_{ij} - m_{kj})^2, \tag{1}$$

where x_{ij} is one of the extracted feature parameters (base line, amplitude, $\tau_{\rm rise}$ and $\tau_{\rm fall}$) of ^{i}th pulse trace, $j = 1, \ldots, 4$, m_{kj} represents the corresponding mean of ^{j}th feature parameter in cluster C_k and is given by

$$m_{kj} = \frac{1}{n_k} \sum_{i \in C_k} \sum_{j=1}^{4} x_{ij}, \tag{2}$$

where n_k is the number of traces in cluster C_k. Figure 4 shows the iteration process to find the minimum of Eq. (1). At the beginning, each trace is assigned to a cluster with a smallest mean, then we calculate the new mean in each cluster. New distance for each trace is then re-calculated and it will be assigned to a cluster with the new smallest mean. The calculation will stop if no trace is assigned to a new cluster.

Typical trace for each cluster is shown in Fig. 5 and the corresponding possible reason is listed in Table 2. Clusters a, e–g are small parts of the total traces and they are rejected. We then correct the baseline for clusters b and c and combine them with cluster d. The histogram of pulse height is plotted in Fig. 6. After rejecting the false traces and correcting the base line, ΔE is improved to 76 eV at 5.9 keV. We found that the K-means clustering algorithm will be effective to reject the false traces if the cluster number and main features are easily identified before the classification.

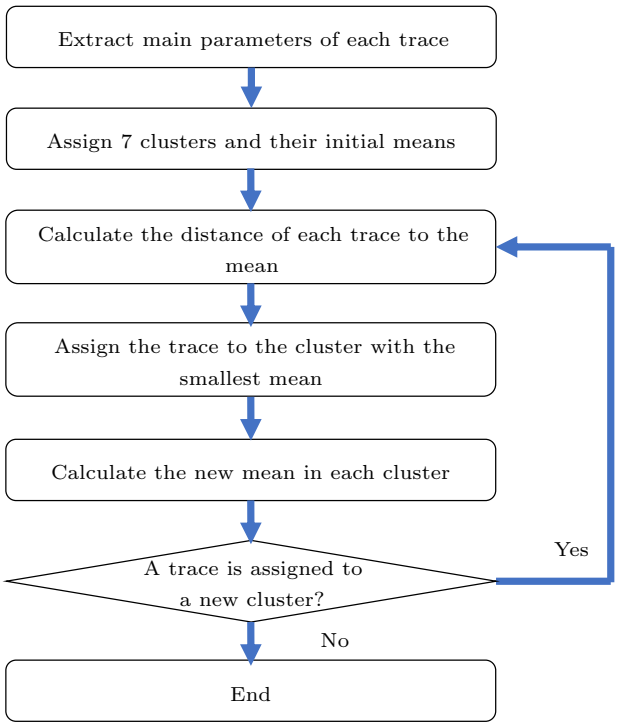


Fig. 4. Flow chart of K-mean clustering.

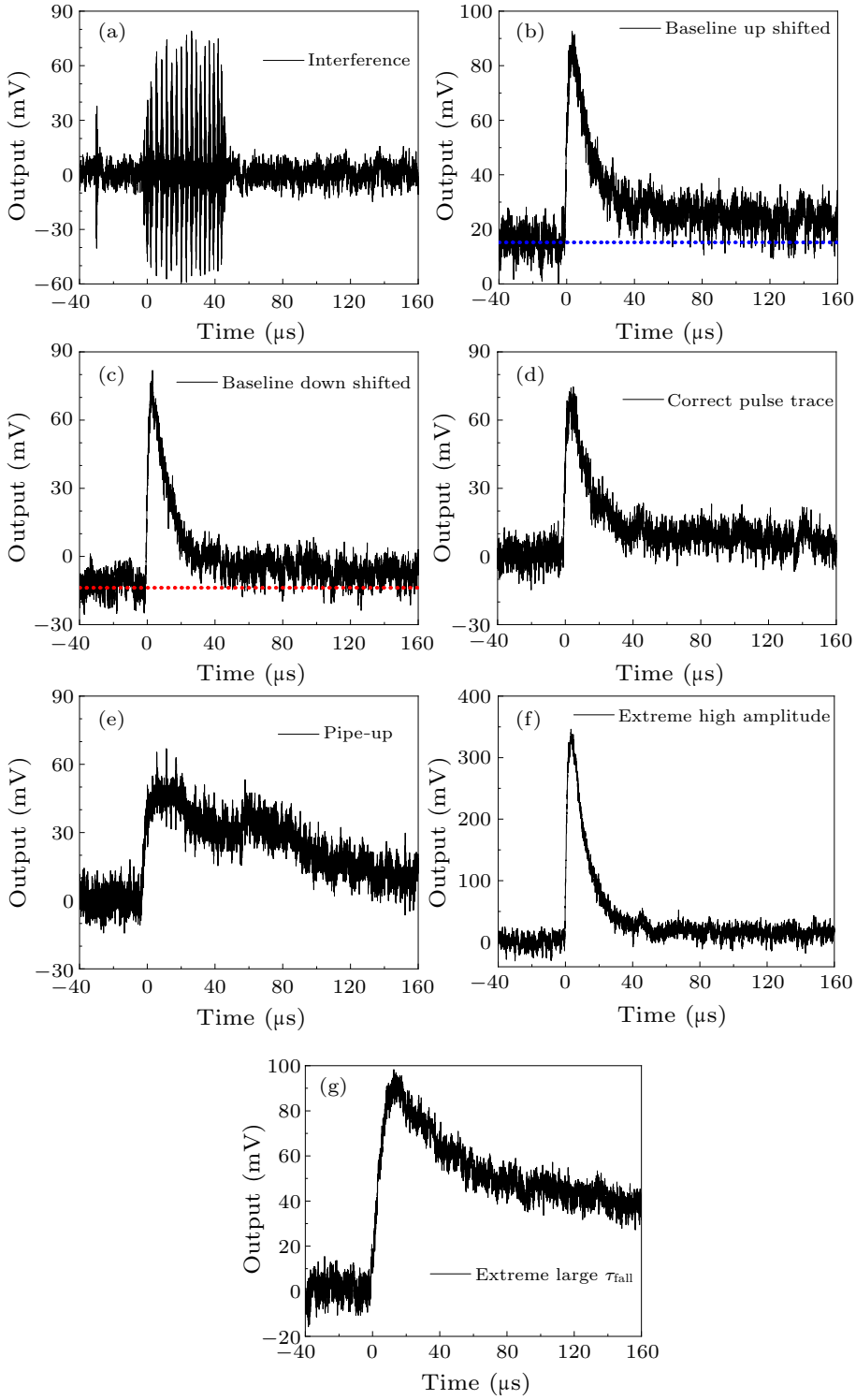


Fig. 5. Typical traces found during the experiment process: (a) interference, (b) baseline up shifted, (c) baseline down shifted, (d) correct pulse trace, (e) pipe-up, (f) extreme high amplitude, (f) extreme large $\tau_{\rm fall}$.

4. Noise reduction using Wiener filter

We further improve the signal-to-noise ratio with Wiener filter.[16] Based on Fig. 6, we choose the pulse traces corresponding to 5.9 keV to obtain the averaged pulses as the template [$S(t)$] (see Fig. 7). The falling time (or effective response time) is about 20 μs, relatively fast in that the silicon substrate is not removed. Each pulse has the form of $H \times S(t)$ since we assume that our superconducting TES detector works in its linear regime, where H is the height (or amplitude) of the pulse trace. Then the pulse height is described as

$$H = \sum D(t) \times S(t), \tag{3}$$

where $S(t)$ is the optimal filtering template, and $D(t)$ the recorded pulse response. The signal-to-noise ratio (SNR) is calculated by

$$\mathrm{SNR} = 20 \log \frac{S}{N}, \tag{4}$$

where S and N represent the signal amplitude and root-mean-square (RMS) noise, respectively. As shown in Fig. 7, after applying the Wiener filter, the SNR is raised from 26 dB to 33 dB. The height distribution as a function of photon energy is shown in Fig. 8, and the obtained ΔE of this TES is 44 eV@5.9 keV.

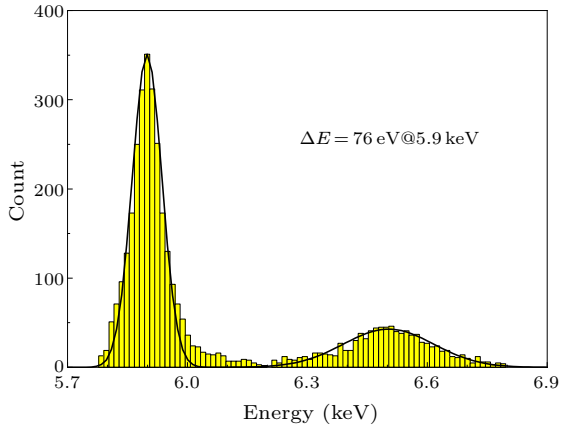


Fig. 6. The energy spectra of x-ray pulses after correcting the baseline.

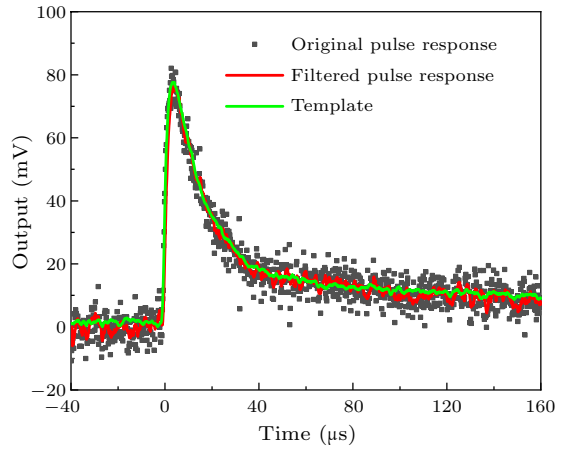


Fig. 7. A typical response before and after Wiener filtering.

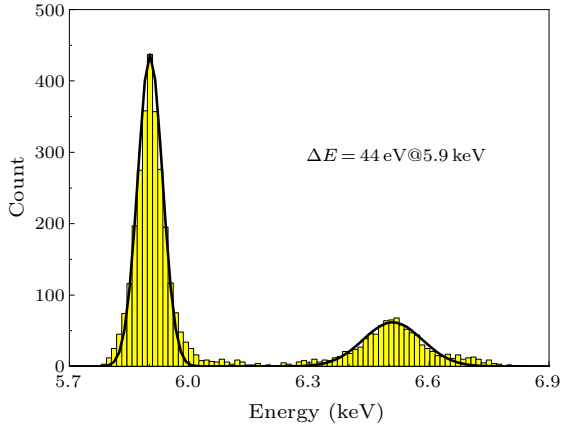


Fig. 8. The energy spectra of x-ray pulses after Wiener filtering.

5. Conclusion

We have studied performance of an x-ray Ti/Au bilayer TES with the Au absorber on the center of the senor without etching the silicon substrate under the sensor. The thermal conductance is 7.7 nW/K, and its recovery time is about 20 μs. By K-means clustering and Wiener filtering, the energy resolution is significantly improved, and it has increased from 94 eV to 44 eV@5.9 keV, which can be further improved by DRIE, reducing T_C by baking,[17] and optimization of the measurement setup.

Acknowledgments

The authors would like to thank Dr. Wentao Wu, Shanghai Institute of Microsystem and Information Technology, for providing the DC SQUID.

Project supported by the National Natural Science Foundation of China (Grant Nos. 12293032, 120101002, 12173097, and U1931123), the National Key Basic Research and Development Program of China (Grant Nos. 2020YFC2201703 and 2018YFA0404701), and Chinese Academy of Sciences (Grant No. GJJSTD20210002).

References

[1] Irwin K D and Hilton G C 2005 *Cryogenic Particle Detection* (Berlin: Springer) pp. 63–150
[2] Barret D, Lam T T, den Herder J W, *et al.* 2016 *Proc. SPIE* **9905** 99052F
[3] Nagayoshi K, Ridder M L, Bruijn M P, Gottardi L, Taralli E, Khosropanah P, Akamatsu H, Visser S and Gao J R 2020 *J. Low Temp. Phys.* **199** 943
[4] Bandler S R, Adams J S, Bailey C N, Busch S E, Chervenak J A, Eckart M E, Ewin A E, Finkbeiner F M, Kelley R L and Kelly D P 2013 *IEEE Trans. Appl. Supercond.* **23** 2100705
[5] Weber J, Morgan K M, Yan D, Pappas C, Wessels A, O'Neil, Bennett D, Hilton G C, Swetz D S, Ullom J N and Schmidt D R 2020 *Superconduct. Sci. Technol.* **33** 115002
[6] Wang H B, Lv Y, Li D X, Zhao Y, GAO B and Wang Z 2023 *Chin. Phys. B* **32** 028501
[7] Zhang S, Xia J K, Sun T, Wu W T, Wu B J, Wang Y L, Cantor R, Han K, Zhou X P, Liu H R, Fan F Y, Guo S M, Liang J C, Li D H, Song Y R, Ju X D, Fu Q and Liu Z 2022 *Nucl. Sci. Tech.* **33** 84
[8] Figueroa-Feliciano E, Cabrera B, Miller A J, Powell S F, Saab T and Walker A 2000 *Nucl. Instrum. Methods Phys. Res. Sect. A* **444** 453
[9] Geng Y 2022 *Characteristics of photon number resolving superconducting transition edge sensors* Ph.D. dessertation (University of Sciences and Technology of China) (in Chinese)
[10] Li P Z, Geng Y, Zhang W, Zhong J Q, Wang Z, Zhou K M, Miao W, Ren Y, Wu F, Zhang K, Yao Q J and Shi S C 2022 *J. Low Temp. Phys.* **209** 248
[11] Muramatsu H, Nahayoshi K, Hayashi T, Sakai K, Yamamoto R, Mitsuda K, Yamasaki N Y, Maehata K and Hara T 2016 *J. Low Temp. Phys.* **184** 91
[12] Wu W T, Lin Z R, Ni Z, Li P Z, Liang T T, Zhang G F, Wang Y L, Ying L L, Peng W, Zhang W, Shi S C, You L X and Wang Z 2022 *Chin. Phys. B* **31** 028504
[13] Hölzer G, Fritsch M, Deutsch M, Hartwig J and Förster E 1997 *Phys. Rev. A* **56** 4554
[14] Lloyd S 1982 *IEEE Trans. Inform. Theor.* **28** 129
[15] Levine, Z H, Gerrits T, Migdall A L, Samarov D V, Calkins B, Lita A E and Nam S W 2012 *J. Opt. Soc. Am. B* **29** 2066
[16] Szymkowiak A E, Kelley R L, Moseley S H and Stahle C K 1993 *J. Low Temp. Phys.* **93** 281
[17] Zhang W, Wang Z, Zhong J Q, Li P Z, Geng Y, Miao W, Ren Y, Zhou K M, Yao Q J and Shi S C 2021 *IEEE Trans. Appl. Supercond.* **31** 2101205